Distribution Agreement

In presenting this thesis as a partial fulfillment of the requirements for a degree from Emory University, I hereby grant to Emory University and its agents the non-exclusive license to archive, make accessible, and display my thesis in whole or in part in all forms of media, now or hereafter now, including display on the World Wide Web. I understand that I may select some access restrictions as part of the online submission of this thesis. I retain all ownership rights to the copyright of the thesis. I also retain the right to use in future works (such as articles or books) all or part of this thesis.

Houston Hartwell Smith April 4, 2018

The Study of Interstellar Ice Analogues

by

Houston Hartwell Smith

Susanna L. Widicus Weaver
Adviser

Chemistry Department

Susanna L. Widicus Weaver

Adviser

Michael C. Heaven

Committee Member

Pat Marsteller

Committee Member

2018

The Study of Interstellar Ice Analogues

By

Houston Hartwell Smith

Susanna L. Widicus Weaver

Adviser

An abstract of
a thesis submitted to the Faculty of Emory College of Arts and Sciences
of Emory University in partial fulfillment
of the requirements of the degree of
Bachelor of Sciences with Honors

Chemistry Department

2018

Abstract

The Study of Interstellar Ice Analogues
By Houston Hartwell Smith

The interstellar medium is an environment that has harsh conditions which can lead to chemical complexity and diversity. Within the interstellar medium, cold molecular cores exist where molecules are both in the gas phase and frozen out on to carbonaceous or silicate grains. Reactions on these grains have been proposed to be a main pathway for the formation of both water and methanol. Methanol has also been proposed to be a starting point for the creation of organic molecules that are biologically relevant, such as amino acids, in an interstellar environment. This work focuses on using mm/sub-mm spectroscopy as a novel technique to detect desorbed molecules from either a thermally processed and/or photoprocessed interstellar ice analogue. The thermal desorption and photofragmentation of methanol were studied, and the results are discussed with a comparison to literature values. The thermal desorption of methanol is approximately 20 K higher than literature values while CO, a desorbed photofragment of a methanol ice, was observed at much higher temperatures than literature values. These temperature discrepancies are discussed within this work. The improvement and optimization of the spectrometer design was completed with the aim of doubling the signal-to-noise (S/N) ratio. However, similar S/N ratios were observed, so further optimization of the spectrometer is needed. When optimized, the increase in S/N ratio will hopefully give more insight into the temperature discrepancies seen from literature values in the thermal processing and photoprocessing of a methanol ice.

The Study of Interstellar Ice Analogues

By

Houston Hartwell Smith

Susanna L. Widicus Weaver

Adviser

A thesis submitted to the Faculty of Emory College of Arts and Sciences
of Emory University in partial fulfillment
of the requirements of the degree of
Bachelor of Sciences with Honors

Chemistry Department

2018

Acknowledgements

I would first like to thank Dr. Widicus Weaver for her four years of mentorship and guidance throughout my time at Emory University. Her mentorship was instrumental in my development as a scientist, and I will be forever grateful for her perspective on science as a whole.

I would also like to thank all the lab members that I have had the pleasure of working with throughout my four years in Dr. Widicus Weaver's lab. Specifically, I would like to thank AJ Mesko for his guidance on the interstellar ice project as well as Luyao Zou for his overall guidance in lab. Next, I am eternally grateful for both Kevin Roenitz and Carson Powers for their help in lab but especially for their friendship outside of lab. Lastly, to all of the other lab members, I thank you for creating a wonderful work environment that made me excited about coming into lab. I wish you all the best with your future endeavors.

Next, I would like to thank both Dr. Heaven and Dr. Marsteller for being on my committee. I am grateful for the time that each of you took to be a part of my committee, and I am honored to have you both review my honor's thesis.

Most importantly, I have to thank my family, specifically my mother and father. You allowed a young boy enthralled by science to explore his dreams by coming to Emory University. I will never be able to repay you for the help and words of encouragement you have given me along the way. The love and guidance you both provide never goes unnoticed. I would also like to thank my girlfriend, Megan Johnson, for her never wavering love and support. Throughout my time at Emory University, you have been a corner stone in my life, and I do not know what I would have done without you.

Table of Contents

Figures

Tables

Introduction:

Approximately 150 years ago, the interstellar medium was thought to be chemically inert and devoid of chemical complexity. However, over the last 150 years of discoveries, the chemistry of the interstellar medium has been shown to be chemically diverse and quite different than the chemistry seen terrestrially. Over this span nearly 200 molecules have been discovered in the interstellar medium ("Molecules in Space," 2018). These molecules range in chemical diversity from H_2 to C_{70} (Cami, Bernard-Salas, Peeters, & Malek, 2010). There are also several unique molecules that aren't present in a terrestrial environment, such as C_7H (Araki et al., 2017; Guelin et al., 1997). Star-forming regions consists of two main environments classified as hot and cold cores. Hot cores range in temperature from 100-300 K and are almost exclusively gas phase molecules (Herbst & van Dishoeck, 2009). However, cold cores are approximately 10-30 K and consist of both gas phase molecules and an icy mantle of molecules frozen out onto silicate or carbonaceous grains (Herbst & van Dishoeck, 2009). These grains are usually 10 nm to 0.5 μm in size, and in dense clouds most of the atoms and molecules adsorb onto them forming a few monolayers of atomic and molecular "ice" (Herbst & van Dishoeck, 2009). A schematic of an interstellar grain is shown in Figure 1, highlighting the physical processes that such a grain would experience in interstellar space. Interstellar grains are exposed to ultraviolet (UV) radiation from either sources internal to the cloud (e.g. embedded protostars or cosmic-ray induced photons) or the diffuse intergalactic radiation field (Greenberg, 1973; Prasad & Tarafdar, 1983; Schutte & Greenberg, 1991; Sternberg, Dalgarno, & Lepp, 1987). Interstellar grains can also be passively heated if a cold core collapses

gravitationally and begins its transition into a hot core star-forming region (Herbst & van Dishoeck, 2009).

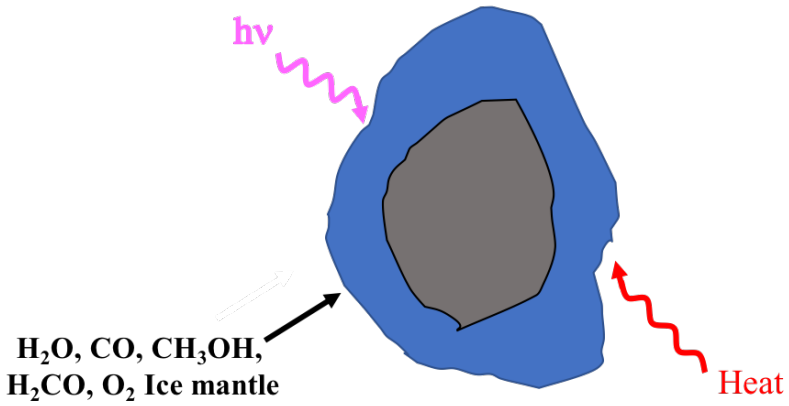

Figure 1: Interstellar ice grain with a variety of molecules that could be frozen onto the surface. Some of the most common molecules are listed, but this is not a comprehensive list. The two processes shown are thermal energy and UV radiation bombardment and are the most prominent in interstellar space.

Ices on interstellar grains were once thought to be limited in chemical complexity due to the extremely low temperatures in dense clouds. It was thought that all the molecules would be locked into place in the ice matrix at 10 K, and hence no chemical reactions would proceed. However, researchers have found that hydrogen atoms are able to move around on grain surfaces at these low temperatures due to quantum tunneling (Cazaux & Tielens, 2002). The high mobility of the hydrogen atoms allows for more complex molecules to form on interstellar grain surfaces. Once star-forming regions begin to heat up past 15 K, even more complicated ice chemistry can occur. Even at cold temperatures, water, H_2O, (Ioppolo, Cuppen, Romanzin, van Dishoeck, & Linnartz, 2008; Miyauchi et al., 2008; Oba et al., 2009) and methanol, CH_3OH, (Fuchs et al., 2009; Hidaka, Watanabe, Shiraki, Nagaoka, & Kouchi, 2004; Hiraoka et al., 2002; Watanabe & Kouchi, 2002) have both been shown through laboratory studies to form from simple precursors like O atoms and CO molecules, respectively. Both of these molecules were studied because they are extremely important to the interstellar medium. Water is the most

abundant molecular species besides H atoms to be deposited on interstellar grains, with a typical fractional abundance of 10^{-4} with respect to H atoms (Herbst & van Dishoeck, 2009). The fractional abundance of water is mostly consistent across different star-forming regions while methanol's fractional abundance is highly variable. The fractional abundance of solid methanol can vary from <1% to 30% with respect to water depending on the source (Herbst & van Dishoeck, 2009). Methanol is particularly important because it is proposed to be the main starting point for the creation of more complicated organic molecules, which can lead to the formation of biologically relevant molecules, e.g. amino acids (Garrod, Widicus Weaver, & Herbst, 2008; Muñoz Caro et al., 2002).

Since both methanol and water have been shown to form on interstellar grains, the next questions to be answered are how these molecules transform when they are either thermally processed and/or photoprocessed. Several scientific articles have been written about the thermal processing of simulated interstellar water ice. Martin-Domenech et al. (2014) found that pure water ice thermally desorbs off a KBr window at 172 K (Martin-Domenech, Muñoz Caro, Bueno, & Goesmann, 2014). Several articles have also been written about the photodesorption and photoproducts of water. However, there are discrepancies in the products produced and in what amounts they are produced. Cruz-Diaz et al. (2018) and Öberg et al. (2009) concluded that O_2, H_2, H_2O, and OH were the species desorbed from a pure water ice during UV photoprocessing (Cruz-Diaz, Martin-Domenech, Moreno, Caro, & Chen, 2018; Karin I. Öberg, Linnartz, Visser, & van Dishoeck, 2009). Both groups also achieved a similar photodesorption yield for H_2O. However, Gerakines et al. (1996) found that HO_2, OH, and H_2O_2 were the main species desorbed (Gerakines, Schutte, & Ehrenfreund, 1996). Due to these

discrepancies, the photodesorption and photolysis of water needs to be further explored to explain these differences.

Methanol ice has also been actively researched over the past 20 years. Martin-Domenech et al. (2014) found that methanol thermally desorbs off a KBr window at 145.2 K (Martin-Domenech et al., 2014). Furthermore, Bertin et al. (2016) found that a pure methanol ice photodesorbs at a rate around 10^{-5} molecules per photon while Cruz-Diaz et al. (2016) placed an upper limit on its rate to be around 10^{-5} molecules per photon (Bertin et al., 2016; Cruz-Diaz et al., 2016). Since Bertin et al. (2016) were able to detect photodesorbed methanol, and Cruz-Diaz et al. (2016) were able to put an upper limit on the same order of magnitude, both studies support the claim that methanol has a photodesorption rate of around 10^{-5} molecules per photon. Bertin et al. (2016) found that if the methanol ice was mixed with CO, the photodesorption rate dropped even further to $<10^{-6}$ molecules per photon (Bertin et al., 2016). Bertin et al. (2016) and Cruz-Diaz et al. (2016) also looked at the photofragments of methanol from methanol photolysis.

The reaction mechanism for methanol photolysis includes the following reactions:

$$CH_3OH + h\nu \rightarrow CH_3O + H \quad (1)$$

$$CH_3OH + h\nu \rightarrow CH_2OH + H \quad (2)$$

$$CH_3OH + h\nu \rightarrow CH_3 + OH \quad (3)$$

$$CH_3OH + h\nu \rightarrow H_2CO + H_2 \quad (4)$$

$$CH_3OH + h\nu \rightarrow HCO + \frac{3}{2}H_2 \quad (5)$$

$$CH_3OH + h\nu \rightarrow CO + 2H_2 \quad (6)$$

Bertin et al. (2016) was able to observe several photofragments including CH_3, OH, CO, H_2CO, and CH_3O/CH_2OH, while Cruz-Diaz et al. (2016) was only able to observe CO and CH_4. Furthermore, Bertin et al. (2016) did not observe methane, CH_4, so there are several discrepancies that need to be investigated further.

The majority of traditional laboratory experiments that simulate and examine interstellar ices use IR spectroscopy to monitor the chemistry of the ice and use mass spectrometry to measure the molecules that desorb from the surface (Cruz-Diaz et al., 2018; Cruz-Diaz et al., 2016; Gerakines et al., 1996; Hidaka et al., 2004; Martin-Domenech et al., 2014; Miyauchi et al., 2008; Moore, Hudson, & Gerakines, 2001; Oba et al., 2009; K. I. Öberg et al., 2009; Karin I. Öberg et al., 2009; Watanabe & Kouchi, 2002). IR spectroscopy is a great tool to monitor solid state chemistry, but certain sections of the IR spectrum, particularly the -OH stretching region, are crowded by overlapping absorption bands that correspond to many molecules which are of interest in astrochemical ices. It requires detailed consideration when assigning these bands to molecules and usually requires isotopic substitutions to distinguish them. Mass spectrometers are incredibly sensitive to trace amounts of molecules but only give the mass of the molecule, so the structure of the molecule cannot be directly gained from the spectrum. As such, new techniques that enable structure-specific detection of species desorbed from interstellar ice analogs are of great value for laboratory astrochemical studies. Rotational spectroscopy, which offers high resolution, high sensitivity, and structure specificity, is ideal for these types of measurements.

During my work in Dr. Widicus Weaver's lab I have implemented a novel spectrometer that uses rotational spectroscopy to study interstellar ice analogs. I have searched for products

liberated into the gas phase from thermal processing and/or photoprocessing of pure water and methanol ices. My goal has been to reproduce some of the results from the above literature using our mm/sub-mm spectroscopic techniques instead of IR spectroscopy and mass spectrometry. Rotational spectroscopy is a novel implementation in this field because most research groups use a combination of IR spectroscopy and mass spectrometry. Our group is utilizing the novel approach of rotational spectroscopy because it is able to directly identify structural properties of gas phase molecules above the ice instead of only obtaining their masses with the mass spectrometer. Our technique allows for a more detailed measurement of desorbed products from the ice and allows for a more complete understanding of molecular life cycles.

Experimental Methods

Two spectrometer designs were constructed and used in the collection of all of the data presented in this thesis. The first spectrometer design was a single-pass frequency-modulated experiment while the second design was a double-pass frequency-modulated experiment. The first spectrometer design is presented in Figure 2 while the second spectrometer design is presented later in the chapter. Figure 3 depicts the side view of both spectrometer designs. Only one schematic is necessary for the side view of the chamber because all of the technical equipment used to construct the spectrometers are the same for both designs except for the equipment on the two flanges omitted. The only difference between spectrometer designs is the far-field optics used to couple the THz light into and out of the chamber which is illustrated

in Figure 2 and Figure 5. For this reason, only one description of the technical equipment will be presented for both designs.

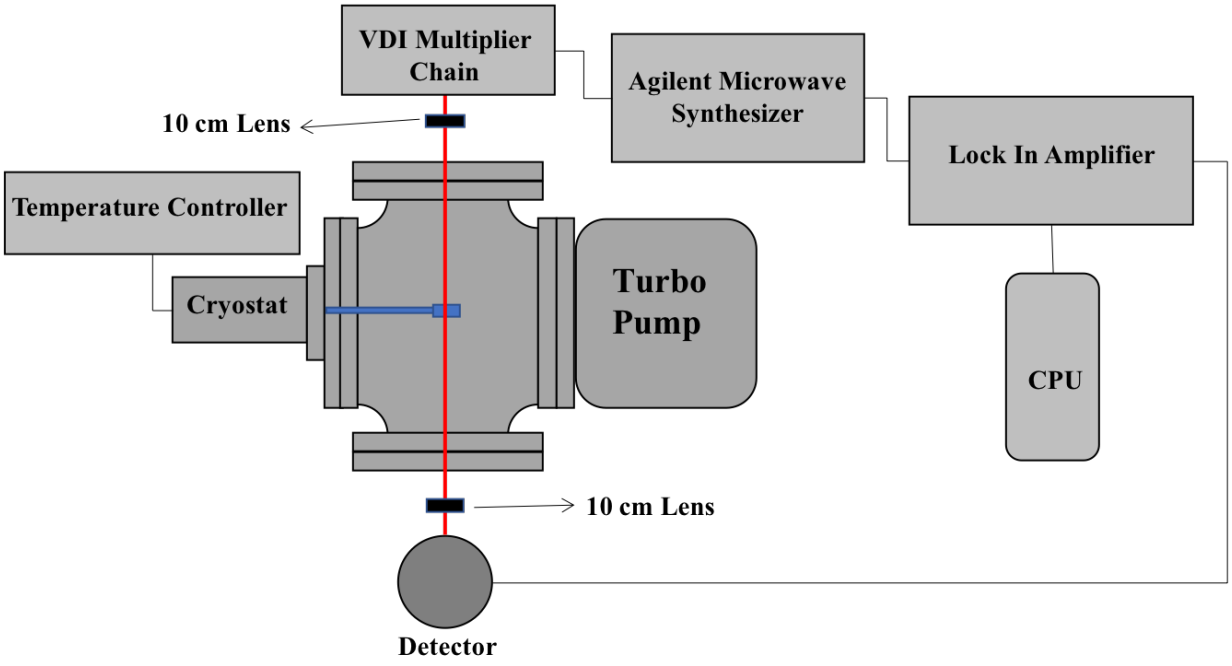

Figure 2: Schematic of a top down view of the single-pass frequency-modulated experiment. The top and bottom flanges are omitted from this schematic for ease of viewing.

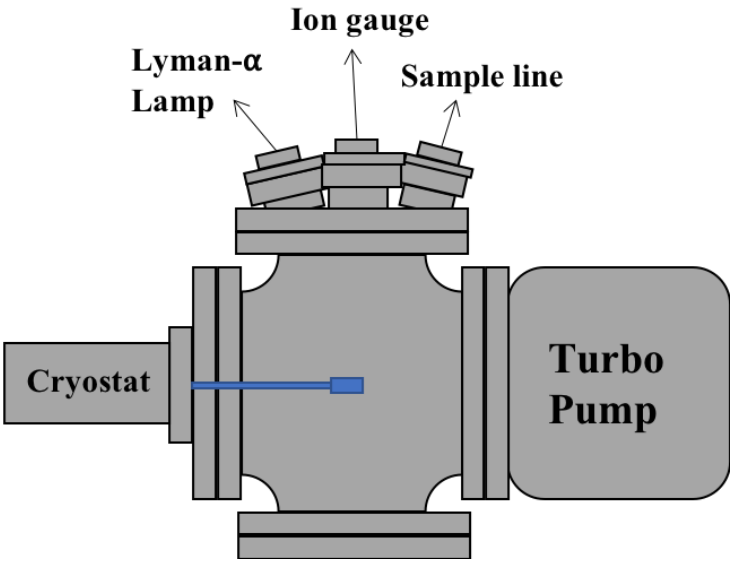

Figure 3: Side view of both single and double pass direct absorption experiments. The two flanges in the plane have been omitted for ease of viewing.

Both spectrometers were constructed in an UHV chamber with six cylindrical ports with an outside diameter (OD) of 8 inches. The spectrometer covers a spectral range from 70-1000 GHz. The base frequency between 23.3 and 37 GHz with a modulation frequency of 1 kHz and a frequency deviation of 75 kHz is generated by an Agilent synthesizer (E8257D). The base frequency is then fed into the Virginia Diodes, Inc., (VDI) multiplier chain (VDI-AMC-s270) via an SMA cable; the frequency of interest is produced via harmonic generation from the input light from the Agilent synthesizer. The VDI system is comprised of several small frequency multipliers that are interchangeable depending on what frequency is needed to scan the molecular transition(s) of interest. A complete guide of all of these components is located in Figure 4.

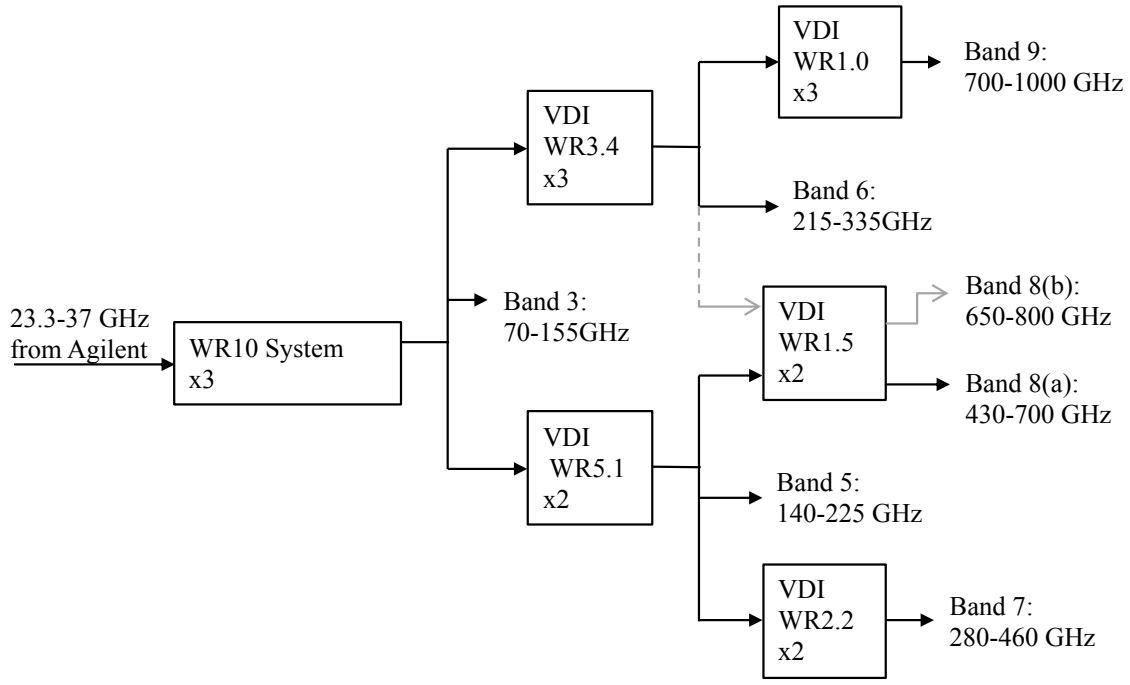

Figure 4: Diagram of frequency multipliers and their specified multiplication and frequency ranges. Diagram modeled after Figure 3 in VDI user guide (Virginia Diodes, 2014).

The output light is then coupled into the chamber via a Teflon lens with a 10-cm focal length. The THz light enters the chamber through a sapphire window, passes over the sample stage,

and exits the chamber through a second sapphire window. Another Teflon lens with a focal length of 10 cm is used to collect the THz light and direct it onto the QMC hot electron bolometer detector (QNbB/PTC). The bolometer sends a voltage that is proportional to the THz signal to the Stanford Research Systems lock-in amplifier (SR830). The Agilent synthesizer also sends a reference frequency of 1.00 kHz with a frequency deviation of 75.00 KHz directly to the lock-in amplifier, which is used for 2f phase-sensitive detection. The lock-in settings are a phase offset of -154.00°, time constant of 10 ms, and a sensitivity of 1 mV for a standard experiment. The output signal from the lock-in is recorded as a function of input frequency by a computer-controlled data acquisition routine.

The double-pass frequency-modulated experiment design, shown in Figure 5, has a THz beam of light that passes through a Teflon lens with a focal length of 10 cm to collimate the beam. The beam is then passed through a Microtech Instruments, Inc. free-standing tungsten ($\rho = 5.28 \times 10^{-8}\ \Omega$ m at 20°C (*Electrical resistivity of pure metals*, 2013), d = 20 μm and g = 50μm) wire grid polarizer. The wire grid is oriented in such a way to allow all the THz light, which has a linear polarization parallel to the surface of the optics table, to be transmitted through. The beam then enters the chamber through a sapphire window, passes over the sample stage, and hits a Newport gold-plated hollow retroreflector (50394-2530). The retroreflector reflects the THz beam back onto itself but rotates the polarization by 90°. The light then passes over the sample stage and out through the sapphire window. The THz beam then comes into contact with the wire grid polarizer. Since the polarization was rotated 90° by the retroreflector, the beam is reflected instead of transmitted through the wire grid polarizer. The wire grid polarizer is set to be at a 45° angle to the THz beam which reflects the polarized THz beam into the

detector. The detector is not sensitive to the polarization of the THz signal, so there is no loss in power due to this change of polarization. However, with this optical setup, the effective path length is doubled which allows for a greater percentage of photons to be absorbed by molecules, and the detected signal is increased.

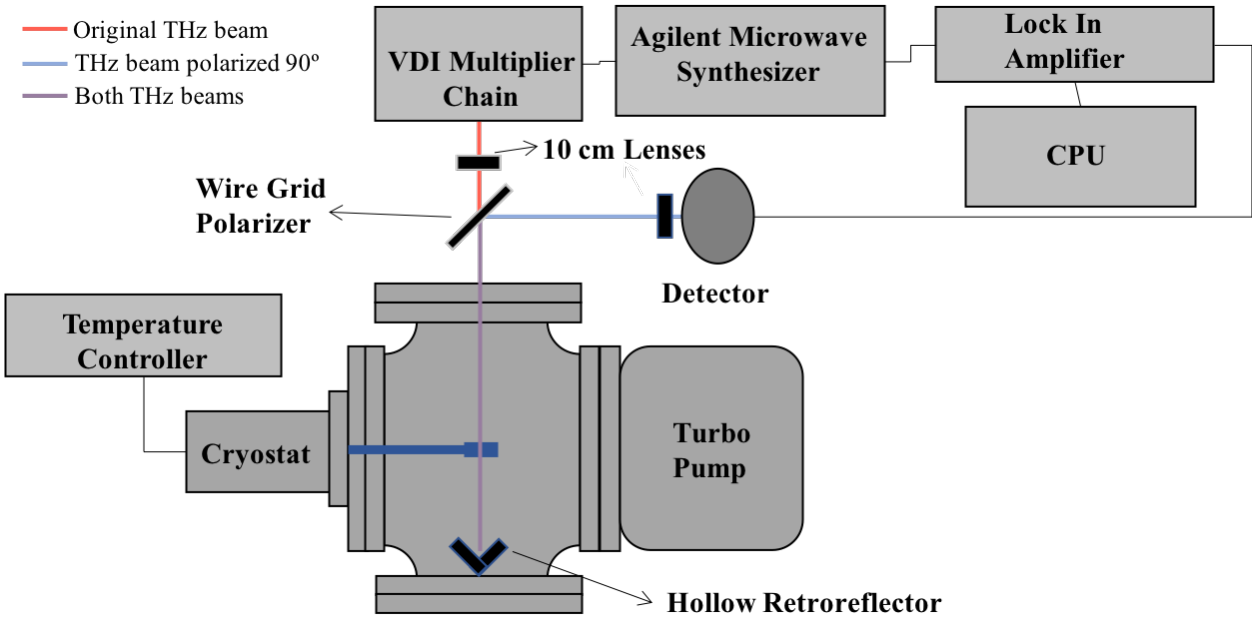

Figure 5: Schematic of a top down view of the double-pass frequency-modulated experiment. The top and bottom flanges have been omitted for ease of viewing.

A crucial part of these spectrometer setups is the sample delivery and manipulation during experiments. The liquid sample is held in an evacuated glass bulb. All samples undergo a freeze-pump-thaw procedure to eliminate any gaseous impurities. The bulb flask has a neck that is continuously being exposed to vacuum once attached. Once the flask valve is opened, the sample evaporates and enters the sample line. The sample line consists of 0.125-inch OD copper tubing equipped with a Matheson high accuracy needle valve (model 4170) for a more refined control of the sample flow rate into the chamber. The aperture of the sample line is located ~0.5 inches above the sample stage. The sample stage is a polished aluminum rectangle

1”x1.5" inches long and is attached to the cold arm. The cold arm is an APD cryogenics expander DE-202B. It is inserted into the center of the chamber and secured by an 8-inch OD flange. The APD cryogenics helium compressor, model HC-2, is connected to the cold arm and cools the stage to ~30 K. The temperature of the sample is adjustable with a Lakeshore model 330 temperature controller. The controller uses a heater attached to the end of the cold arm and a thermocouple temperature gauge on the bottom of the sample stage to regulate the temperature. Throughout most experiments temperatures will vary from 30-300 K depending on the sample. Another important aspect of sample manipulation is the use of the Opthos Instruments static Lyman-α lamp as a continuous source of UV photons. The lamp is angled directly above the sample stage. An Opthos Instruments Evenson cavity is used to sustain a plasma discharge in the lamp throughout the duration of photolysis experiments. The plasma discharge is microwave induced by an Opthos Instruments microwave generator.

Baseline pressure for the system is approximately 1.0×10^{-7} Torr. This high vacuum pressure is achieved with the use of a Leybold turbo drive 700 molecular vacuum pump backed by an Edward's E2M18 rotary vane vacuum pump. The high vacuum pressure is measured with a Duniway model I-CFF-275 hot ion gauge filament pressure gauge. The rough vacuum pressure is measured with a Leybold Thermovac transmitter model TTR 91.

Results and Discussion

Improvement and Optimization of the Interstellar Ice Project

During the past two years, I have improved the overall baseline pressure from 4.0×10^{-7} Torr to 1.0×10^{-7} Torr by creating a better vacuum seal between vacuum components. The optics,

according to the first spectrometer design, were optimized to improve alignment for the experiment. The QMC hot electron bolometer detector (QNbB/PTC) was implemented into the spectrometer design during this time. Before the change to the QMC (QNbB/PTC) bolometer, a QMC (QFI/2BI) was used. A signal-to-noise (S/N) ratio experiment was performed on gaseous CH_3OH with a static chamber pressure of ~$3.0x10^{-2}$ Torr. Four separate spectral absorption lines of CH_3OH were recorded for each bolometer and appear in Figure 6. The "signal" was calculated by taking the signal at the center of the absorption peak and subtracting it from the baseline signal while the standard deviation of a portion of the background was used for the noise. The lock-in sensitivity, phase offset, and modulation frequency were different for each detector. The sensitivity was at 5 mV, phase offset of 80.00°, and a modulation frequency of 15 kHz for the QFI/2BI detector and sensitivity of 50 mV, phase offset of -154.00°, and modulation frequency of 1 kHz for the QNbB/PTC detector.

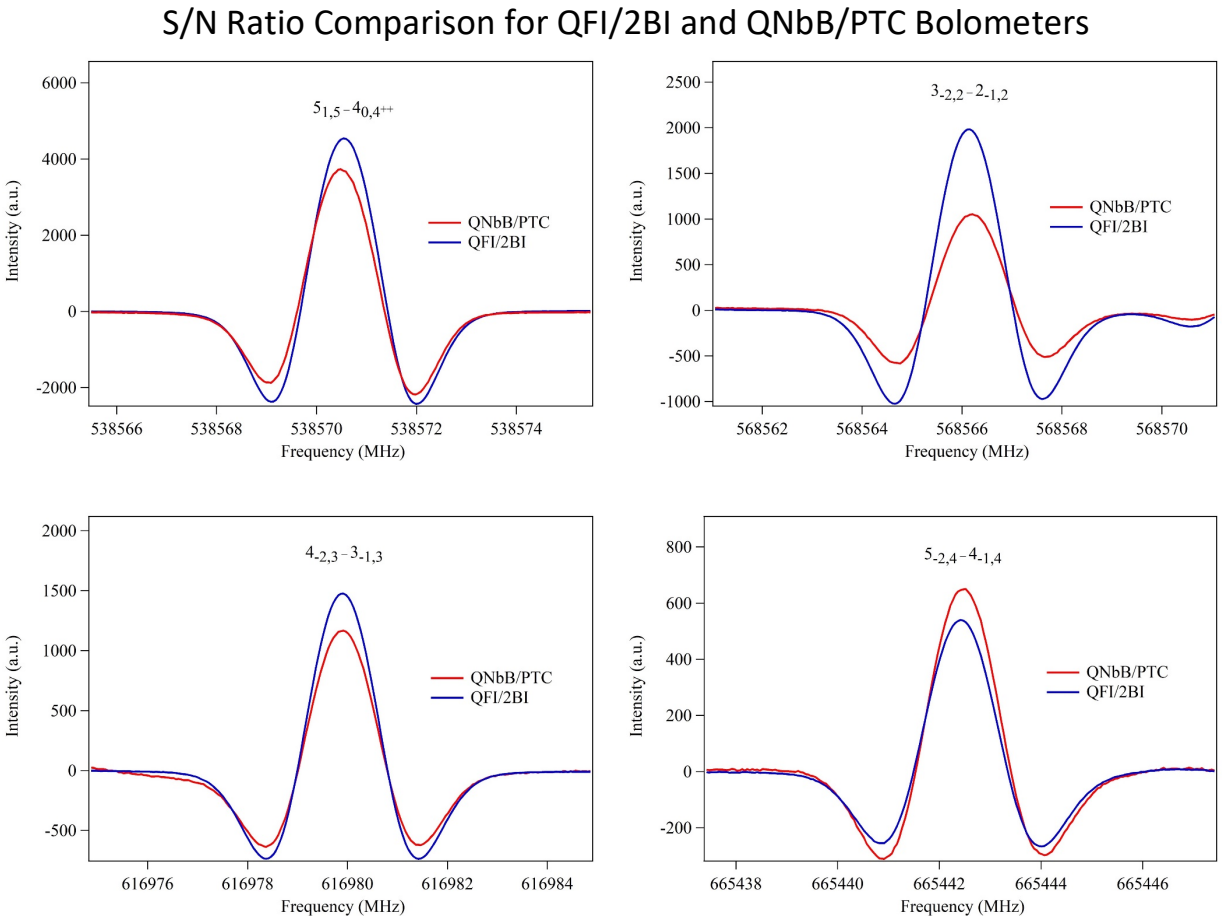

Figure 6: Four separate CH_3OH lines with center frequencies of 538570.58 MHz, 568566.05 MHz, 616979.98 MHz, and 665442.45 MHz are shown. Each spectrum has 20 averages. No spectrum was boxcar smoothed so that a true S/N ratio could be calculated. The quantum numbers for the molecular transition are labelled above the signal's peak.

Since the sensitivity is not the same for both bolometers the intensities of each CH_3OH peak are not an accurate depiction of its overall strength. However, since the S/N ratio is only a ratio of the signal to noise, the spectra can be compared on the same plot without correcting for intensity. The QNbB/PTC model has approximately an order of magnitude higher signal than the QFI/2BI bolometer, but the QNbB/PTC also has approximately one order of magnitude higher

spectral noise. S/N ratios for each CH_3OH line recorded by both bolometers are shown in Table 1.

Table 1: S/N ratio for four CH_3OH lines for the QNbB/PTC and QFI/2BI Bolometers

Bolometer Model	538570 MHz	568566 MHz	616979 MHz	665442 MHz
QNbB/PTC	646	393	75	308
QFI/2BI	674	1096	566	344

The QNbB/PTC model has a slightly lower S/N ratio for both the 538570 MHz and 665442 MHz lines while it has a significantly smaller S/N ratio for the 568566 MHz and 616979 MHz lines. The difference in signal to noise between both bolometers is frequency dependent based off of Table 1, but it can be assumed that the QNbB/PTC model is comparable to the QFI/2BI model. Thus, the QNbB/PTC model was used for the results presented in this thesis.

Simulated CH_3OH Ice

The first simulated CH_3OH ice experiment was to record the signal of CH_3OH molecules thermally desorbing off a solid CH_3OH ice. At the start of the experiment, the base pressure was $1.2x10^{-7}$ Torr, and the gate valve to the turbo was closed to begin the sample deposition. The CH_3OH sample, Sigma-Aldrich HPLC grade CH_3OH, was frozen out at approximately 40 K under static pumping conditions with a sample dosing pressure of $1.20x10^{-3}$ Torr for three minutes. The chamber was then evacuated back to a baseline pressure before the gate valve was reclosed. Subsequently, the CH_3OH ice was warmed using a temperature programmed desorption (TPD) technique under static pumping conditions. This technique involves the temperature being increased in a linear stepwise manner and held constant at certain temperatures to record a spectrum before resuming the stepwise increase. The linear increase

was set at a rate of 2 K/min up until 100 K then a rate of 1 K/min was used. The CH_3OH TPD was performed with the single-pass frequency-modulated spectrometer design, and a spectrum was recorded every 10 K up until 160 K where a spectrum was recorded every 5 K. These increments were chosen because it minimizes the number of scans required to detect a thermal desorption event without ramping past it. A selection of thermal desorption spectra of CH_3OH are shown in Figure 7. The pressure for the spectrum taken at 160 K is 9.0×10^{-5} Torr, and the pressure for the spectra at 165 K and 170 K is ~2.3×10^{-3} Torr. This pressure spike is indicative of a substantial number of molecules entering the gas phase.

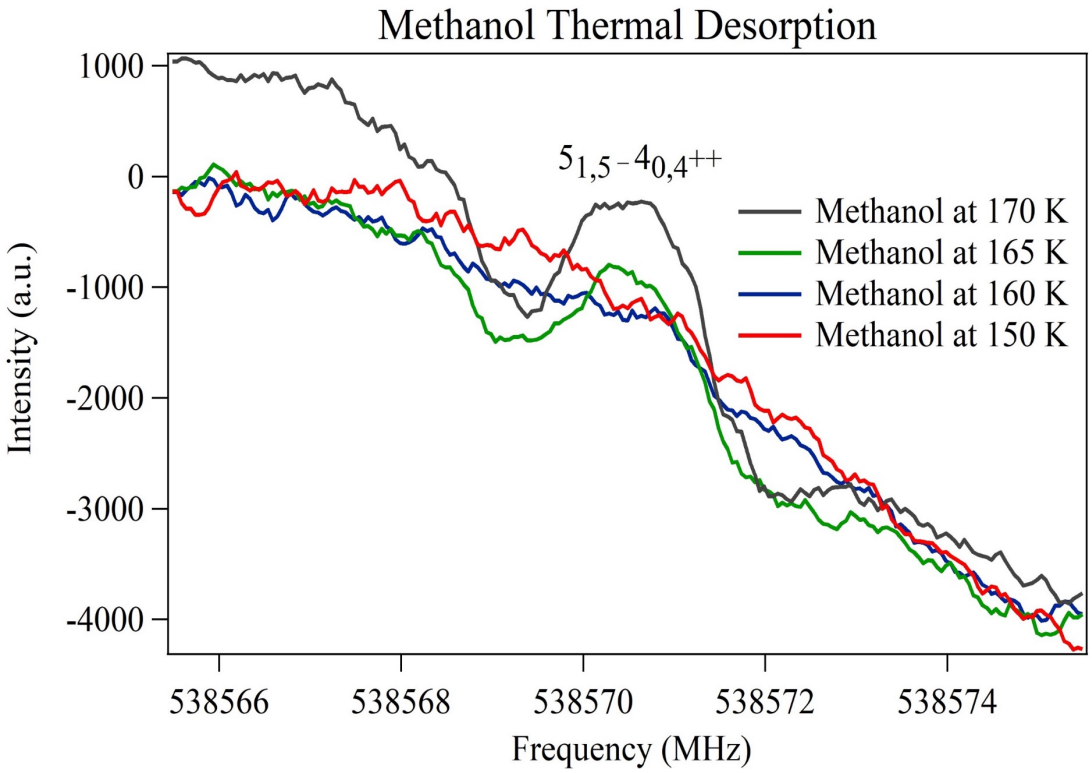

Figure 7: CH_3OH thermal desorption spectrum recorded at 150, 160, 165, and 170 K. Each spectrum was boxcar smoothed x6. The quantum numbers for the molecular transition are labelled above the signal's peak.

Figure 7 also corroborates the idea that a substantial number of molecules entered the gas phase because there is an increase in signal from the CH_3OH spectrum taken at 160 K to

that taken at 170 K. Based on these two different verification methods, there is a clear indication that CH_3OH is desorbing off the aluminum stage and entering the gas phase. However, our observed temperature is approximately 20 K higher than the literature value of 145.2 K (Martin-Domenech et al., 2014). There are several possibilities for this difference, including inaccurate temperature calibration, difference in solid ice phase, or contamination of the chamber. The inaccuracy of the temperature controller was ruled out because it was calibrated several months before these measurements were taken. The phases of the ice should have been similar because CH_3OH has no phase changes between ~10 K for the Martin-Domenech et al. (2014) experiment and ~40 K for this experiment. However, the contamination of the sample cannot be ruled out because we have no way of determining the composition of the newly formed ice.

Once the gate valve is closed to the turbo pump to begin the sample deposition, water from the walls of the chamber could degas and enter the gas phase. If the cold stage is at 40 K, the gaseous water molecules will deposit a layer of water ice onto the cold stage before the desired sample is deposited. Unfortunately, a water transition was not monitored during the above experiment, but a water line was monitored during the photolysis and subsequent warm-up of a CH_3OH ice. The photolysis experiment occurred several days after the CH_3OH TPD experiment and the chamber was not opened to atmosphere in between these experiments. Since the chamber was not opened to atmosphere, the water contamination present in the photolysis experiment would have been present in the CH_3OH TPD experiment. All of the experimental conditions and spectrometer design were held constant for both the thermal and photoprocessed CH_3OH ice experiments except for the sample deposition and the irradiation

with a static Lyman-α lamp. For the photoprocessing experiment, the sample was deposited for three minutes and ten seconds with a pressure of 1.0×10^{-5} Torr. The Lyman-α lamp irradiated the CH_3OH ice for five minutes at 40 K before being turned off. Spectra of CO, CH_3OH, and H_2O were also taken every 2 K instead of 5 K for a finer temperature resolution.

An increase in absorption signal around water's center frequency is indicative of water present in the gas phase between 160 K and 170 K. These temperatures are around water's thermal desorption temperature of 172 K. (Martin-Domenech et al., 2014). The spectra of water contamination at various temperatures are shown in Figure 8.

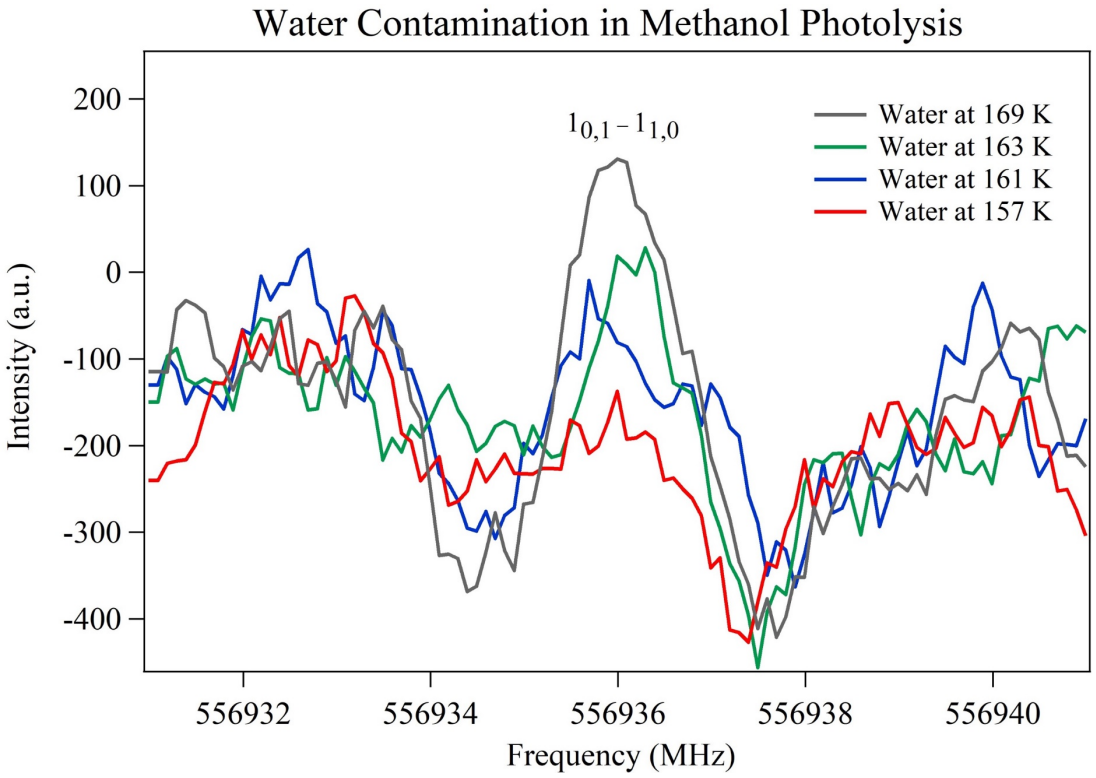

Figure 8: Water contamination observed around its thermal desorption temperature during the warm-up of a photoprocessed CH_3OH ice. Each spectrum was boxcar smoothed x6. The quantum numbers for the molecular transition are labelled above the signal's peak.

Both cited literature values for water and CH_3OH's thermal desorption are the peak temperatures of their TPD curves, but these curves extend and show desorption 10 to 15 K on

either side of this peak temperature. Thus, it is within reason to assume our experimental thermal desorption temperature of water is accurate, but the thermal desorption temperature of CH_3OH is still slightly out of range.

One reason for this discrepancy could be due to the CH_3OH ice forming atop a small water ice contamination layer. Since the CH_3OH is adhered to the water ice, it is hypothesized to have a stronger dipole-dipole interaction with water than the aluminum substrate. The stronger dipole-dipole interaction causes the CH_3OH ice to sublime only once the temperature is high enough to sublime the water ice. The above explanation is plausible, but the composition and phase of the ice need to be determined to make a definitive conclusion. Since neither of those questions can be directly identified in this experimental design, a definitive answer cannot be given for the discrepancies in temperature from literature values.

We also conducted experiments to detect a photoproduct of a photoprocessed CH_3OH ice during this warm-up period to try and replicate the research by Bertin et al. (2016) and Cruz-Diaz et al. (2016). CO was chosen as the photoproduct to search for as it has the highest photodesorption rate of all photoproducts including photodesorbed CH_3OH (Bertin et al., 2016). Spectra of CO ranging in temperature from 249 K to 274 K are shown in Figure 9.

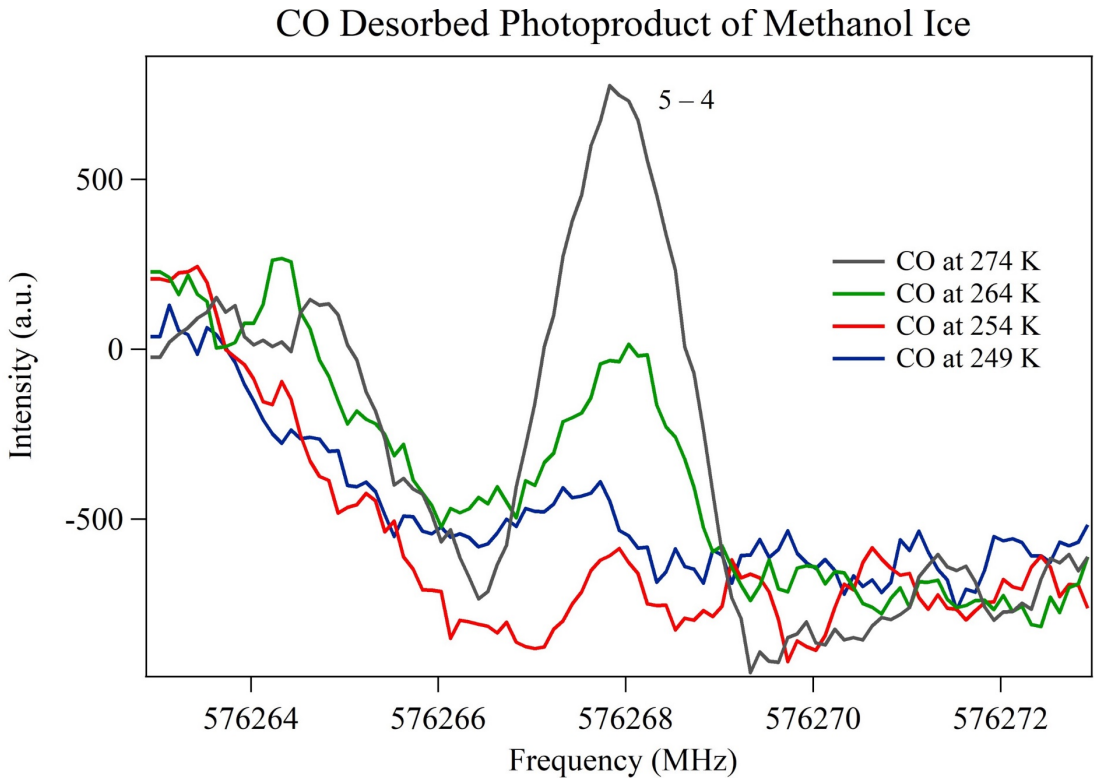

Figure 9: Spectra of CO from a photoprocessed CH_3OH from 249-274 K. Each spectrum was boxcar smoothed x6. The quantum numbers for the molecular transition are labelled above the signal's peak.

The temperature at which we see CO desorption is extremely high compared to a pure CO ice at 29.9 K (Martin-Domenech et al., 2014). Martin-Domenech et al. (2014) also showed that if CO is mixed with other molecules such as H_2O and CH_3OH, it will continually desorb off the ice mixture after its thermal desorption temperature. This is in stark contrast to our experiment where CO isn't seen until 254 K.

An explanation for this dramatic difference is that when CO molecules are desorbed from the cold stage, they are redepositing farther up the cold arm before a sufficient number density can be detected by our mm/sub-mm rotational spectroscopy. This redeposition is possible because the electrical heater is located at the end of the cold arm near the aluminum stage while the whole cold arm is cooled by a closed-loop helium compressor. Once the

aluminum stage is at its base temperature, the cold arm has 3 other “stages” or sections not including the cold stage at different temperatures. The temperatures for each “stage” in order from farthest to closet to the aluminum stage are around 200 K, 100 K, and 50 K respectively. The sections farther from the aluminum stage are not affected as drastically during the warm-up process which means the temperature for these sections could be below the temperature needed to redeposit H_2O and CH_3OH molecules. The stages are too warm for CO molecules to adsorb since CO desorbs at ~30 K on a pure CO ice, but it could adsorb onto H_2O or CH_3OH ice at higher temperatures due to dipole-dipole interactions. If H_2O or CH_3OH adsorb onto any section of the cold arm, a CO molecule could then adsorb onto this newly formed ice. As the temperature is continually increased, all the sections of the cold arm reach a temperature higher than the desorption temperature for this ice mixture which causes the molecules attached to the cold arm to completely sublime. The temperature trend with CO was also observed with H_2O and is shown in Figure 10. Due to both H_2O and CO having the same trends, the above explanation is viable because a higher number density of H_2O and CO are seen at these higher temperatures than at their reported thermal desorption temperatures.

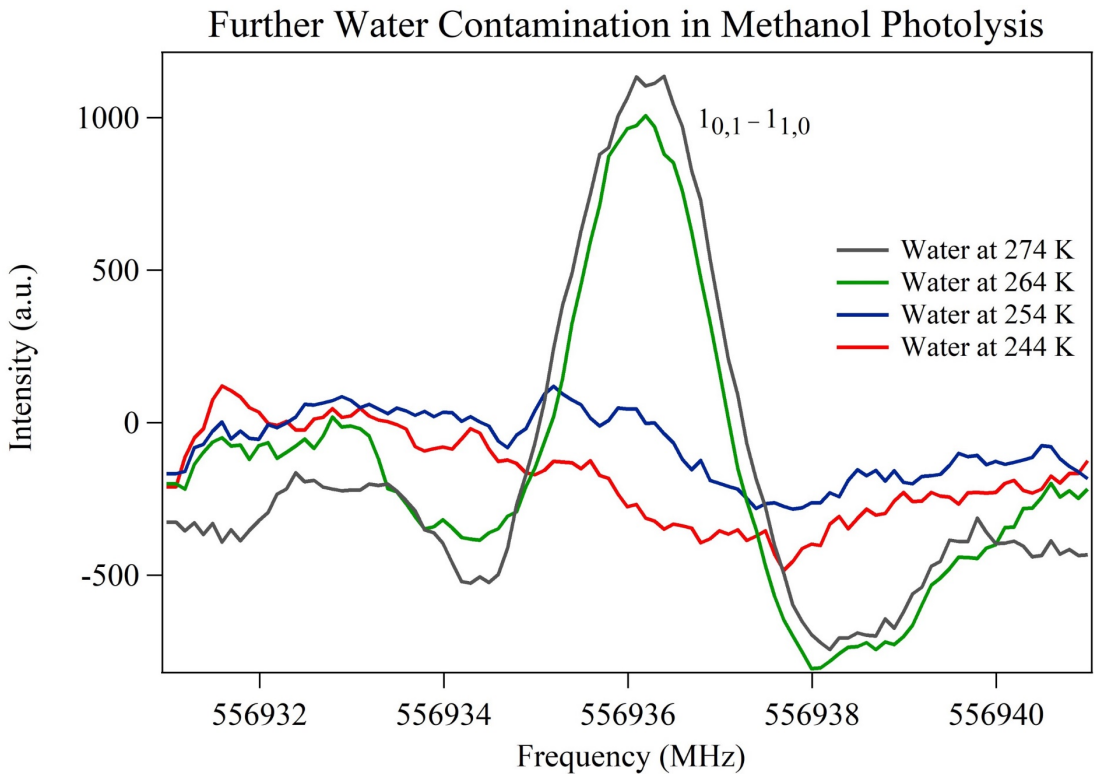

Figure 10: Water contamination observed above its thermal desorption temperature during the warm-up of a photoprocessed CH_3OH ice. Each spectrum was boxcar smoothed x6. The quantum numbers for the molecular transition are labelled above the signal's peak.

A spectrometer design with a greater detection sensitivity than our first design was sought to determine if the proposed explanation is plausible. The double-pass frequency-modulated spectrometer design was created to increase detection sensitivity to gain a better understanding of this increased desorption temperature issue.

Double-pass Spectrometer Design and Pressure Sensitivity Measurements

The second spectrometer design (see Figure 5) is a double-pass frequency-modulated design with the aim to increase the sensitivity of our detection by a factor of 2. The new spectrometer was constructed as shown in Figure 5, and the pressure sensitivity of the spectrometer was measured with a gaseous water experiment at room temperature, T = 298 K. For this experiment the chamber was continuously pumped by the turbo pump. The baseline

pressure for this experiment was $3.0x10^{-7}$ Torr, and a background water spectrum was recorded at this pressure. The high accuracy needle valve was slowly opened until the desired pressure was reached and then a spectrum of water was taken. The pressure was monitored, and the needle valve was opened more or less to keep a constant pressure throughout the scan. Several different chamber pressures of water were scanned: $5.2x10^{-7}$ Torr, $7.5x10^{-7}$ Torr, $1.3x10^{-6}$ Torr, and $3.0x10^{-6}$ Torr. Figure 11 illustrates all of these spectra overlaid to show the increase in signal.

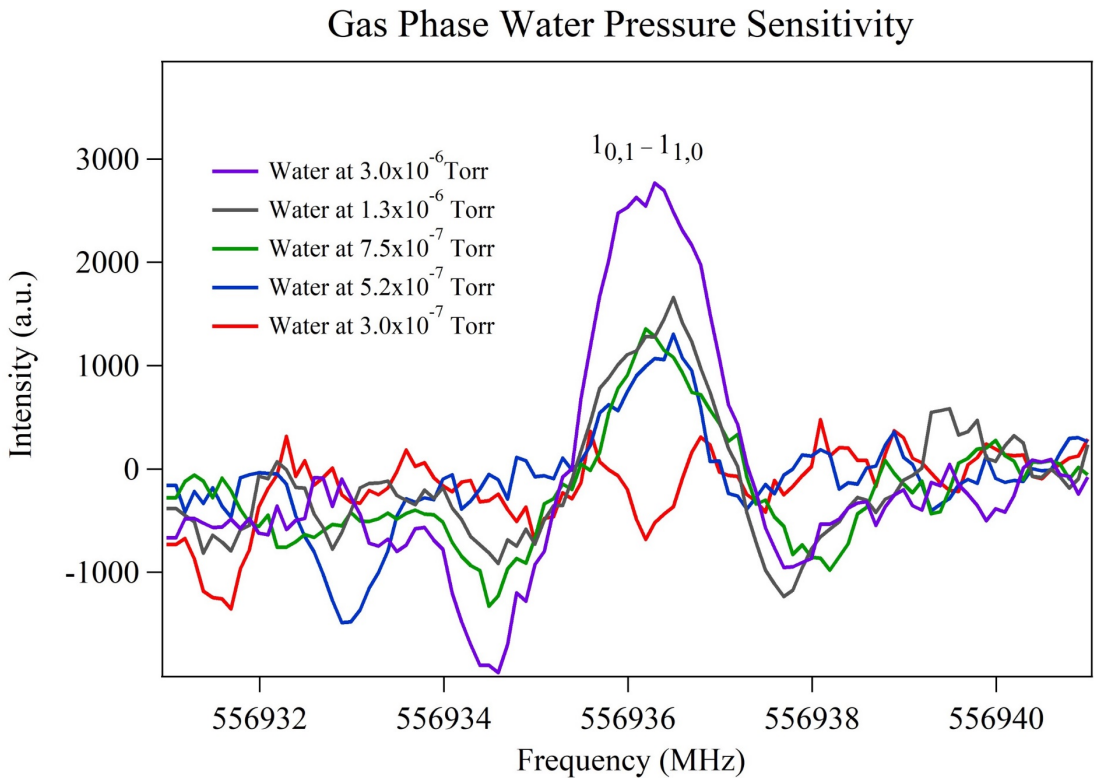

Figure 11: Overlaid water spectra at various pressures at room temperature, T = 298 K. Each spectrum was boxcar smoothed x6. The quantum numbers for the molecular transition are labelled above the signal's peak.

From this experiment, we detected water at a lower pressure limit of $5.2x10^{-7}$ Torr. An approximate number density can be calculated from the simple ideal gas law, PV = nRT. Based on the ideal gas law, a number density of $1.7x10^{10}$ molecules cm^{-3} was detected. Since the baseline pressure of $3.0x10^{-7}$ Torr isn't solely water, we were able to detect a lower partial

pressure of water than 5.2×10^{-7} Torr. However, 5.2×10^{-7} Torr was used because it is a definitive upper limit of the pressure needed to detect water.

For a signal-to-noise (S/N) ratio comparison to the previous, single-pass design, two spectra with approximately the same pressure were overlaid and examined. These two spectra are presented in Figure 12.

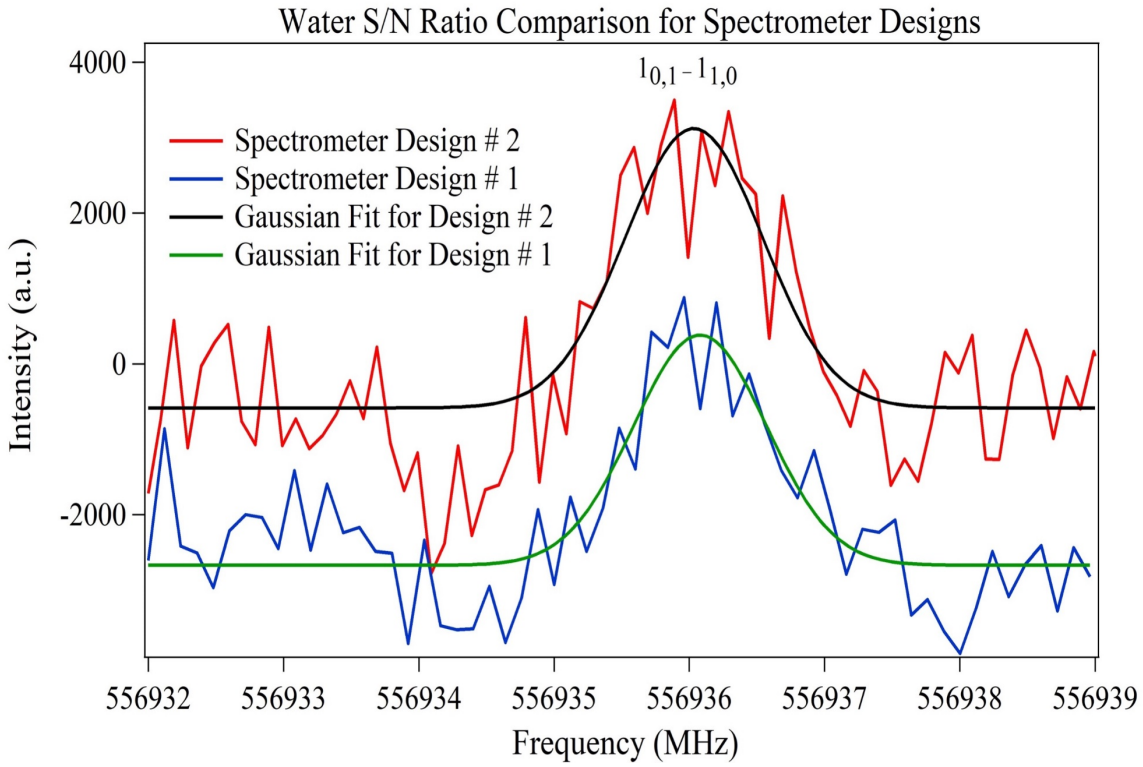

Figure 12: S/N ratio comparison between both spectrometer designs at approximately the same pressure and at room temperature, T = 298 K. The Spectrometer Design # 1 has a y-offset applied, so that it can be visually compared to Spectrometer Design # 2. No boxcar smoothing was applied so that a true S/N ratio could be calculated. The quantum numbers for the molecular transition are labelled above the signal's peak.

The pressure for the first design is 4.0×10^{-6} Torr, and the pressure for the second design is 3.0×10^{-6} Torr. The spectrum for the first design was taken in 2016, and it had the same optical configuration of the spectrometer design used for all the CH_3OH ice experiments. The new spectrometer design depicted in Figure 5 was implemented in the spring of 2018. One

assumption in this comparison is that both the QNbB/PTC and QFI/2FI bolometers have approximately the same S/N ratio at this frequency. This comparison is not an exact parallel but is only used to qualitatively examine the difference between both spectrometer designs. A Gaussian function was fit to each spectrum due to the low amount of signal observed. The "signal" was calculated by taking the peak of the Gaussian function and subtracting it from the baseline of this function. The standard deviation of a portion of the spectrum where there was no signal was used for noise in the calculation of S/N ratio. The spectra gave a comparable S/N ratio of ~5.9 and ~4.8 for the first and second spectrometer designs, respectively. However, the spectrum for the first design had 16 averages while the second design had 10. Since the S/N ratio ideally increases proportionally to the square root of the number of averages, the first design has a $\sqrt{\frac{16}{10}}$ increase in S/N ratio over the second design. To account for this increase, the second design can be multiplied by $\sqrt{\frac{16}{10}}$ which intern gives a S/N = 6.0 if it had 16 averages. Ideally the second spectrometer design would increase the S/N ratio by a factor of 2 since it is doubling the effective path length of the system. The reason for the lack of improvement is unclear, but it is likely related to optical alignment. The optical configuration is currently being optimized in the hopes of repeating the gas phase water test and seeing the S/N ratio increase by a factor of 2 over the first spectrometer design. Once this is achieved, proof of concept experiments with thermal desorbed and photodesorbed water will be performed to compare our results with literature values. This increase in S/N ratio will hopefully help us elucidate the differences in desorption temperatures of CO, and CH_3OH.

Conclusion:

I have summarized the research I performed in Dr. Widicus Weaver's lab throughout my time at Emory University. During my research time, I have focused on advancing the scientific knowledge gained from the interstellar ice project as well as the optimization of this experiment. Since interstellar ices are hypothesized to be where prebiotic molecules could form in star-forming regions, they are inherently important to simulate in a laboratory environment to explore the possible reaction mechanisms that form these molecules (Garrod et al., 2008). Of these interstellar ices, both water and CH_3OH ices are the most vital to understand due to water's ubiquity in the interstellar medium and CH_3OH's importance in forming prebiotic molecules.

I was able to advance the scientific knowledge of the experiment by simulating pure methanol ices and performing either thermal processing and/or photoprocessing experiments. The aim of these experiments was to confirm certain important literature information with a novel technique, i.e. using mm/sub-mm rotational spectroscopy to monitor the desorbed molecules above a simulated methanol ice. Two main discrepancies with literature values were seen during these experiments. The first discrepancy was that the thermal desorption of methanol was ~20 K higher than previously reported literature (Martin-Domenech et al., 2014). This difference was explored and hypothesized to be caused by a small contamination of water ice formed on the cold stage. The second discrepancy was the desorption temperature of CO being extremely high compared to previously reported data (Martin-Domenech et al., 2014). This result was also thoroughly investigated and hypothesized to result from a redeposition event farther up the cold arm during the warm-up process. This hypothesis was supported by

observing higher abundances of water between 249 K and 274 K than at its thermal desorption temperature.

To elucidate these temperature differences from literature values, the double-pass frequency-modulated spectrometer design was created and implemented into the experiment with the aim of increasing the S/N ratio by a factor of 2. The spectrometer design was implemented and shown to have a gaseous water pressure sensitivity of 5.2×10^{-7} Torr which correlates to an approximate number density of 1.7×10^{10} molecules cm^{-3}. The S/N ratio comparison between both spectrometer designs showed that they were approximately equivalent, so further optimization of the optical configuration for the second spectrometer design needs to be performed to achieve the factor of 2 increase. However, once implemented this increase in S/N ratio will hopefully help elucidate the discrepancies in desorption temperature of both CH_3OH and CO.

References

Araki, M., Takano, S., Sakai, N., Yamamoto, S., Oyama, T., Kuze, N., & Tsukiyama, K. (2017). Long Carbon Chains in the Warm Carbon-chain-chemistry Source L1527: First Detection of C7H in Molecular Clouds. *Astrophysical Journal, 847*(1), 7. doi:10.3847/1538-4357/aa8637

Bertin, M., Romanzin, C., Doronin, M., Philippe, L., Jeseck, P., Ligterink, N., . . . Fillion, J.-H. (2016). UV PHOTODESORPTION OF METHANOL IN PURE AND CO-RICH ICES: DESORPTION RATES OF THE INTACT MOLECULE AND OF THE PHOTOFRAGMENTS. *Astrophysical Journal Letters, 817*(2). doi:10.3847/2041-8205/817/2/l12

Cami, J., Bernard-Salas, J., Peeters, E., & Malek, S. E. (2010). Detection of C-60 and C-70 in a Young Planetary Nebula. *Science, 329*(5996), 1180-1182. doi:10.1126/science.1192035

Cazaux, S., & Tielens, A. (2002). Molecular hydrogen formation in the interstellar medium (vol 575, pg 29, 2002). *Astrophysical Journal, 577*(2), L127-L127. doi:10.1086/344385

Cruz-Diaz, G. A., Martin-Domenech, R., Moreno, E., Caro, G. M. M., & Chen, Y. J. (2018). New measurements on water ice photodesorption and product formation under ultraviolet irradiation. *Monthly Notices of the Royal Astronomical Society, 474*(3), 3080-3089. doi:10.1093/mnras/stx2966

Cruz-Diaz, G. A., Martin-Domenech, R., Munoz Caro, G. M., & Chen, Y. J. (2016). Negligible photodesorption of methanol ice and active photon-induced desorption of its irradiation products. *Astronomy & Astrophysics, 592*. doi:10.1051/0004-6361/201526761

Electrical resistivity of pure metals. (2013). In W. M. Haynes (Ed.), *CRC Handbook of Chemistry and Physics*.

Fuchs, G. W., Cuppen, H. M., Ioppolo, S., Romanzin, C., Bisschop, S. E., Andersson, S., . . . Linnartz, H. (2009). Hydrogenation reactions in interstellar CO ice analogues A combined experimental/theoretical approach. *Astronomy & Astrophysics, 505*(2), 629-639. doi:10.1051/0004-6361/200810784

Garrod, R. T., Widicus Weaver, S. L., & Herbst, E. (2008). Complex chemistry in star-forming regions: An expanded gas-grain warm-up chemical model. *Astrophysical Journal, 682*(1), 283-302. doi:10.1086/588035

Gerakines, P. A., Schutte, W. A., & Ehrenfreund, P. (1996). Ultraviolet processing of interstellar ice analogs .1. Pure ices. *Astronomy & Astrophysics, 312*(1), 289-305.

Greenberg, J. M. (1973). *Molecules in the Galactic Environment* (L. E. S. M.A. Gordon Ed.). New York: John Wiley & Sons ltd. .

Guelin, M., Cernicharo, J., Travers, M. J., McCarthy, M. C., Gottlieb, C. A., Thaddeus, P., . . . Saito, S. (1997). Detection of a new linear carbon chain radical: C7H. *Astronomy & Astrophysics, 317*(1), L1-L4.

Herbst, E., & van Dishoeck, E. F. (2009). Complex Organic Interstellar Molecules. *Annual Review of Astronomy and Astrophysics, Vol 47, 47*, 427-480. doi:10.1146/annurev-astro-082708-101654

Hidaka, H., Watanabe, N., Shiraki, T., Nagaoka, A., & Kouchi, A. (2004). Conversion of H2CO to CH3OH by reactions of cold atomic hydrogen on ice surfaces below 20 K. *Astrophysical Journal, 614*(2), 1124-1131. doi:10.1086/423889

Hiraoka, K., Sato, T., Sato, S., Sogoshi, N., Yokoyama, T., Takashima, H., & Kitagawa, S. (2002). Formation of formaldehyde by the tunneling reaction of H with solid CO at 10 K revisited. *Astrophysical Journal, 577*(1), 265-270. doi:10.1086/342132

Ioppolo, S., Cuppen, H. M., Romanzin, C., van Dishoeck, E. F., & Linnartz, H. (2008). LABORATORY EVIDENCE FOR EFFICIENT WATER FORMATION IN INTERSTELLAR ICES. *Astrophysical Journal, 686*(2), 1474-1479. doi:10.1086/591506

Martin-Domenech, R., Muñoz Caro, G. M., Bueno, J., & Goesmann, F. (2014). Thermal desorption of circumstellar and cometary ice analogs. *Astronomy & Astrophysics, 564*, 12. doi:10.1051/0004-6361/201322824

Miyauchi, N., Hidaka, H., Chigai, T., Nagaoka, A., Watanabe, N., & Kouchi, A. (2008). Formation of hydrogen peroxide and water from the reaction of cold hydrogen atoms with solid oxygen at 10 K. *Chemical Physics Letters, 456*(1-3), 27-30. doi:10.1016/j.cplett.2008.02.095

Molecules in Space. (2018).

Moore, M. H., Hudson, R. L., & Gerakines, P. A. (2001). Mid- and far-infrared spectroscopic studies of the influence of temperature, ultraviolet photolysis and ion irradiation on cosmic-type ices. *Spectrochimica Acta Part a-Molecular and Biomolecular Spectroscopy, 57*(4), 843-858. doi:10.1016/s1386-1425(00)00448-0

Muñoz Caro, G. M., Meierhenrich, U. J., Schutte, W. A., Barbier, B., Segovia, A. A., Rosenbauer, H., . . . Greenberg, J. M. (2002). Amino acids from ultraviolet irradiation of interstellar ice analogues. *Nature, 416*(6879), 403-406.

Oba, Y., Miyauchi, N., Hidaka, H., Chigai, T., Watanabe, N., & Kouchi, A. (2009). FORMATION OF COMPACT AMORPHOUS H2O ICE BY CODEPOSITION OF HYDROGEN ATOMS WITH OXYGEN MOLECULES ON GRAIN SURFACES. *Astrophysical Journal, 701*(1), 464-470. doi:10.1088/0004-637x/701/1/464

Öberg, K. I., Garrod, R. T., van Dishoeck, E. F., & Linnartz, H. (2009). Formation rates of complex organics in UV irradiated CH3OH-rich ices I. Experiments. *Astronomy & Astrophysics, 504*(3), 891-U828. doi:10.1051/0004-6361/200912559

Öberg, K. I., Linnartz, H., Visser, R., & van Dishoeck, E. F. (2009). PHOTODESORPTION OF ICES. II. H2O AND D2O. *Astrophysical Journal, 693*(2), 1209-1218. doi:10.1088/0004-637x/693/2/1209

Prasad, S. S., & Tarafdar, S. P. (1983). UV-RADIATION FIELD INSIDE DENSE CLOUDS - ITS POSSIBLE EXISTENCE AND CHEMICAL IMPLICATIONS. *Astrophysical Journal, 267*(2), 603-609. doi:10.1086/160896

Schutte, W. A., & Greenberg, J. M. (1991). EXPLOSIVE DESORPTION OF ICY GRAIN MANTLES IN DENSE CLOUDS. *Astronomy & Astrophysics, 244*(1), 190-204.

Sternberg, A., Dalgarno, A., & Lepp, S. (1987). COSMIC-RAY-INDUCED PHOTODESTRUCTION OF INTERSTELLAR-MOLECULES IN DENSE CLOUDS. *Astrophysical Journal, 320*(2), 676-682. doi:10.1086/165585

Virginia Diodes, I. (2014). VDI USER GUIDE. In.

Watanabe, N., & Kouchi, A. (2002). Efficient formation of formaldehyde and methanol by the addition of hydrogen atoms to CO in H(2)O-CO ice at 10 K. *Astrophysical Journal, 571*(2), L173-L176. doi:10.1086/341412